MIT Open Access Articles

Torque Measurement With Compliant Mechanisms

Massachusetts Institute of Technology

Torque Measurement With Compliant Mechanisms

Raymond Ma

Alexander H. Slocum, Jr.

Edward Sung

Precision Compliant Systems Laboratory,
Department of Mechanical Engineering,
Massachusetts Institute of Technology,
Cambridge, MA 02139

Jonathan F. Bean
Harvard Medical School,
Department of Physical Medicine and Rehabilitation,
Spaulding Cambridge Outpatient Center,
Cambridge, MA 02138

Martin L. Culpepper
Precision Compliant Systems Laboratory,
Department of Mechanical Engineering,
Massachusetts Institute of Technology,
Cambridge, MA 02139

This work focuses on the design, development, and testing of an inexpensive, low-profile, cartwheel flexure mechanism for torque measurement. It has been designed primarily for use in a rehabilitation and diagnostics instrument for the treatment of ankle injuries. The sensor is manufactured rapidly and at low-cost using an $Omax^{TM}$ abrasive waterjet machine. Strain gauges are bonded to the flexure beams to measure applied strain using a full wheatstone bridge circuit. Displacement, force, and torque are then calculated from the measured circuit voltage; power and velocity can also be determined if required by the application. Experimental results show that there exists a linear relationship between applied torque and output voltage of the wheatstone bridge for the nested cartwheel flexure design. Furthermore, results of preliminary tests of an ankle rehabilitation device show that it fulfills a need not currently satisfied by current rehabilitation and diagnostic technology in physical medicine and rehabilitation.
[DOI: 10.1115/1.4023326]

1 Introduction

Accurate torque measurement is critical in feedback systems and measurement devices utilizing revolute joints. Many existing torque sensors and transducers use magneto-elastic materials to measure torsional strain in a central cylinder to determine applied torque. Some biomechanical applications, however, require sensors with a low-profile, e.g., the ankle rehabilitation device discussed herein. The cartwheel flexures presented here were developed as part of a machine created to measure the dynamic capabilities of the human ankle joint complex (AJC), shown in Fig. 1.

The device is currently undergoing clinical tests evaluating its efficacy to diagnose, evaluate, and rehabilitate ankle injuries [1,2]. Given the relatively low torque output and finite range of motion (ROM) of the ankle joint, high end torque sensors are not cost-effective. Flexure-based torque sensors with adequate ROM provide patients with a more gradual and less painful method of joint evaluation and mitigate risk of damage to injured joints.

A well-designed flexure provides accurate, repeatable, and predictable motion with the use of a low-maintenance mechanism at a relatively low cost [3,4]. Systematic practices for designing flexure systems has been developed for a variety of applications [4], including mechanisms for measurement and actuation at the nanoscale [5]. The linear relationship between strain and applied load makes cartwheel flexures better suited for measurement of the human ankle joint.

2 Methods

The design of cartwheel flexures applies existing principles of force sensor design to torque measurement. An analysis of the motions of these compliant mechanisms was presented by Pei et al., who proposed a pseudorigid-body model validated by nonlinear finite element analysis (FEA) [6]. Another consideration of cartwheel flexures began with a simple fixed-guided beam model [7]. The building block of a cartwheel flexure is assumed to be a fixed-guided beam, with a first-order validation performed using COSMOSWORKS^{TM}. The use of off-the-shelf components, combined with the ease of manufacture of cartwheel flexures with abrasive waterjet machines highlights the cost-effectiveness and simplicity of the design.

Circumferentially arranged single flexure blades were proposed by Vischer and Khatib in the early 1990s; the mechanism was utilized for torque feedback control in a prototype robotic linkage [8]; however, inductive transducers were used instead of strain gauges. Later work sought to improve upon the design by decreasing the spatial requirements of integrating the components in robotic systems [9] and further decreasing the sensitivity of the mechanism to radial forces [10]. The majority of current ring-shaped torque sensors are complex and thus costly to manufacture.

A fixed-guided beam is the basic building block of a cartwheel flexure, as shown in Fig. 3; Eq. (1) gives the relationship between load and deflection for this mechanism

$$\delta = \frac{FL^3}{3EI} \qquad (1)$$

When arranged circumferentially with the inner "race" fixed to ground and a torque applied to the outer "race," the flexures
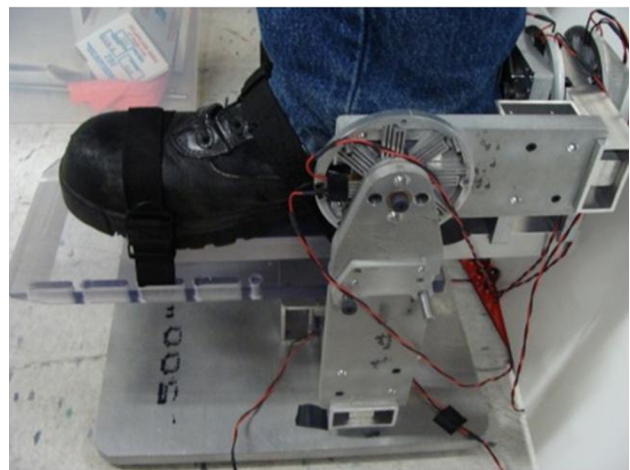

Fig. 1 Ankle rehabilitation device utilizing cartwheel flexures as torque sensors
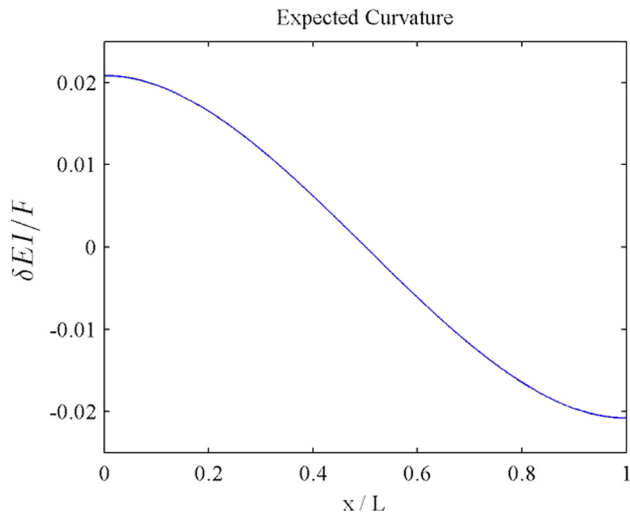
Expected Curvature

Fig. 2 Simplified model of flexure deformation

$$\delta(x) = \frac{1}{EI}\left[\frac{P}{12}x^3 - \frac{PL}{8}x^2 + \frac{PL^3}{48}\right] \qquad (2)$$

undergo axisymmetric deflection [11] as can be seen in Fig. 2. This is repeatable as long as the flexure does not plastically deform.

The flexural beams in the cartwheel flexure approximately behave as two such modified beams joined together. The close-form equation for these modified cantilever beams can be derived by assuming that the system acts as a skew-symmetric system, assuming that the moment and deflection are both zero at the mid-point. Under those assumptions, the analytical solution for beam deflection is shown in Eq. (2)

2.1 Cartwheel Flexure Design. The relative motion between the inner and the outer rim results in deformation in the beams, and imparts a measurable strain in the flexures, as illustrated in Fig. 3. When implemented as an interface between two components in relative motion, the flexure acts as a revolute joint with a range of motion and rotational stiffness determined by material selection and flexure geometry.

A benefit of the cartwheel flexure is that it can be integrated into the machine structure. These sensors can be manufactured cost-effectively and rapidly to within tolerances of 0.005″ on a commercial waterjet machine. The cartwheel flexures used here are cut from a 6.35 mm (0.25 in.) thick sheet of 6061-T6 aluminum. Mounting holes were machined directly into the inner and outer races of the flexure.

Work done by Trease et al. [12] suggests that compliant mechanisms suffer from axis drift and lack of off-axis stiffness. These two parasitic motions prevent the center of rotation from remaining fixed, and subject the mechanism to parasitic motions in undesired directions, respectively. The symmetric design of the cartwheel flexure serves to mitigate axis drift. Trease et al. proposed a new flexure-based design for a revolute joint that, while minimizing aforementioned errors, requires a more complicated manufacturing process and more space to achieve the same performance.

2.2 Flexure Calibration. The cartwheel flexure must be properly calibrated to ensure an accurate measurement of the applied load. Calibration was accomplished using the circuit
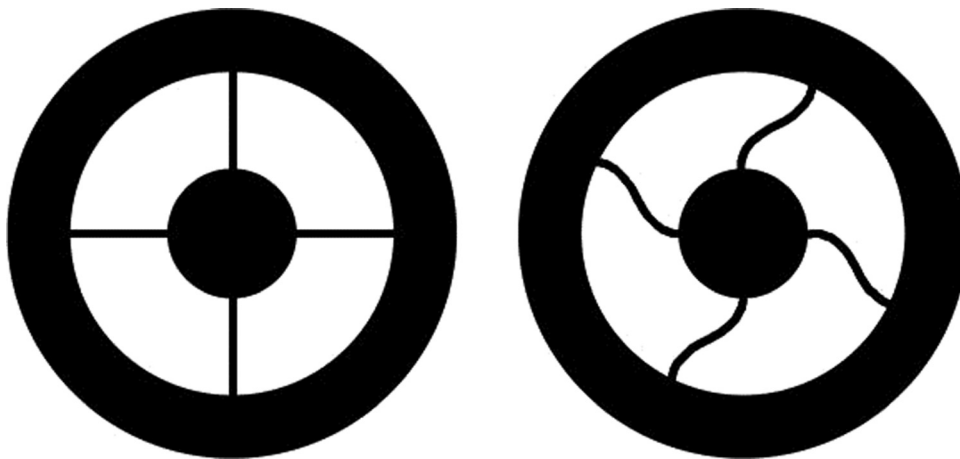

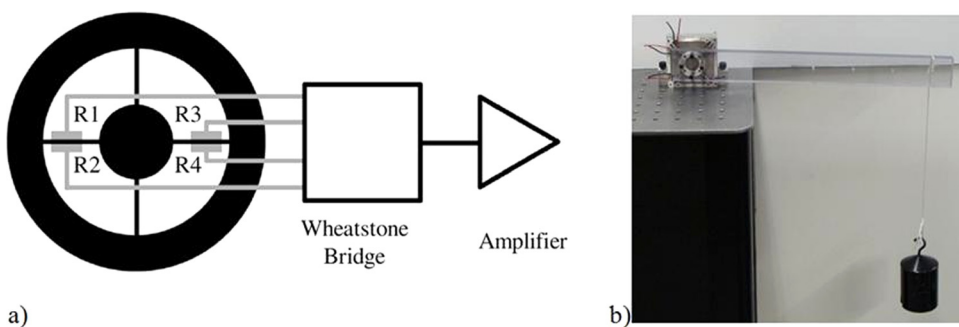**Fig. 3 Cartwheel flexure deformation**

Fig. 4 (a) Schematic of cartwheel flexure circuit; (b) calibration setup utilizing weights to apply a known, repeatable torque to the cartwheel flexure
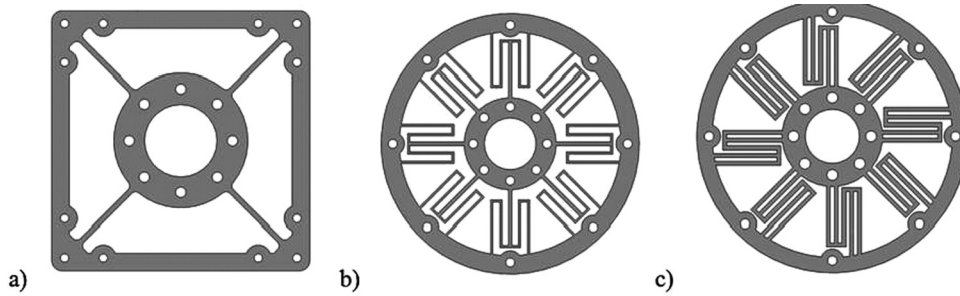
Fig. 5 Cartwheel flexure designs

Table 1 Expected deformation and maximum torque load of different cartwheel flexure designs

Parameter	Design 1	Design 2	Design 3
Flexure thickness (mm)	1.27	0.762	0.762
Maximum torque (Nm)	7	22	55
Maximum radial displacements (rad)	0.015	0.065	0.054

shown in Fig. 4(*a*) and the experimental setup shown in Fig. 4(*b*). By applying torque through calibrated weights hung from a beam fixed to the inner ring an accurate force/deflection relationship could be measured. It should be noted that the outer ring was

grounded to an optical table to mitigate the effects of vibration errors on the measurement.

2.3 Flexure Optimization. To adjust stiffness or compliance, the topology and the arrangement of the flexure blades, in addition to their length and thickness, can be modified. This can be accounted for using simulation software such as COSMOWORKS^TM, especially when a closed-form relationship between torque and strain is too cumbersome or complicated to calculate. Finite element analysis can then be used to determine the maximum allowable torque before the flexure blades suffer from hysteresis.

SolidWorks^TM solid models of the three cartwheel flexure designs are shown in Fig. 5, and were used in past robotic systems
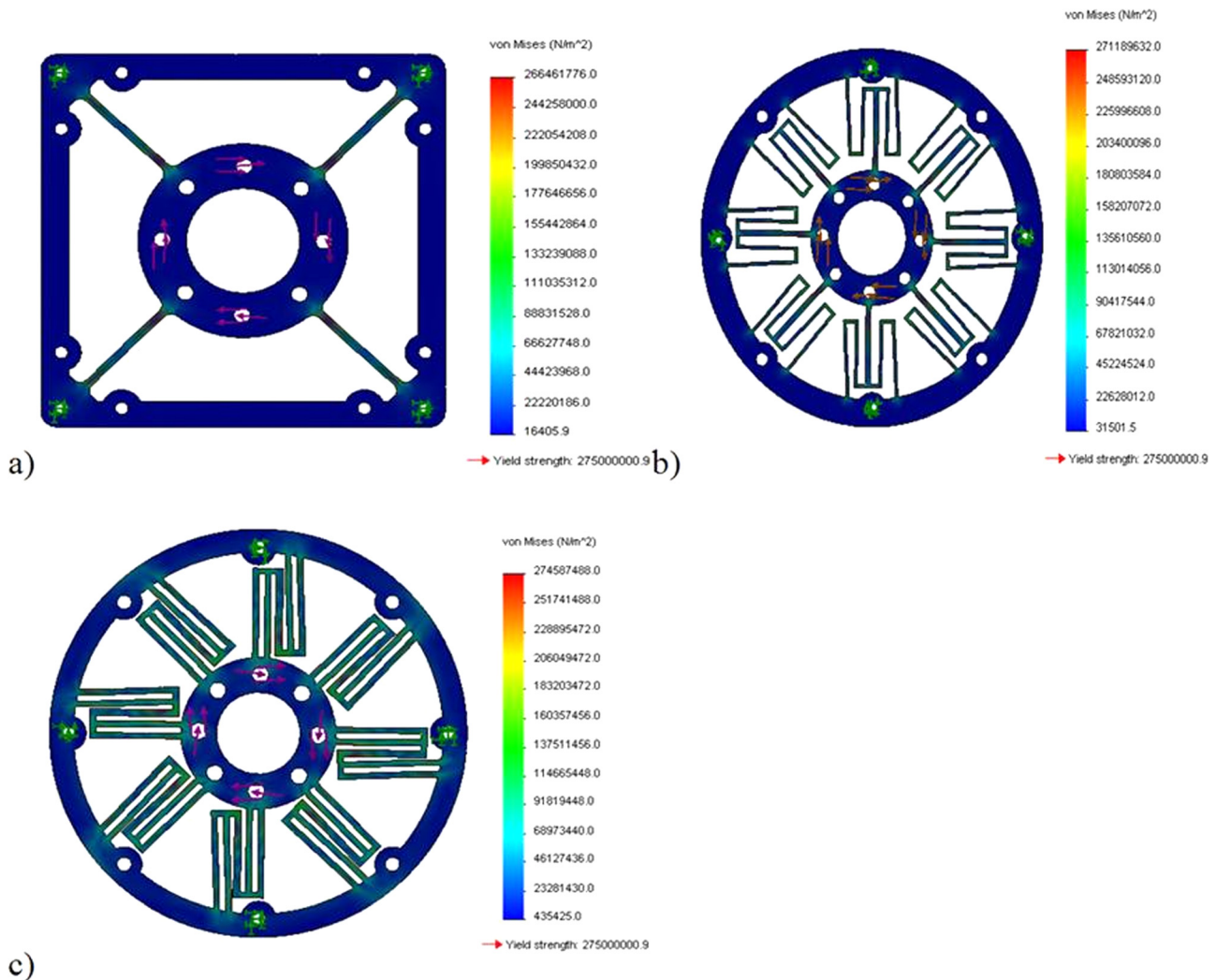

Fig. 6 FEA results for cartwheel flexure designs (*a*) one; (*b*) two, with increased ROM; and (*c*) three, with increased load capacity
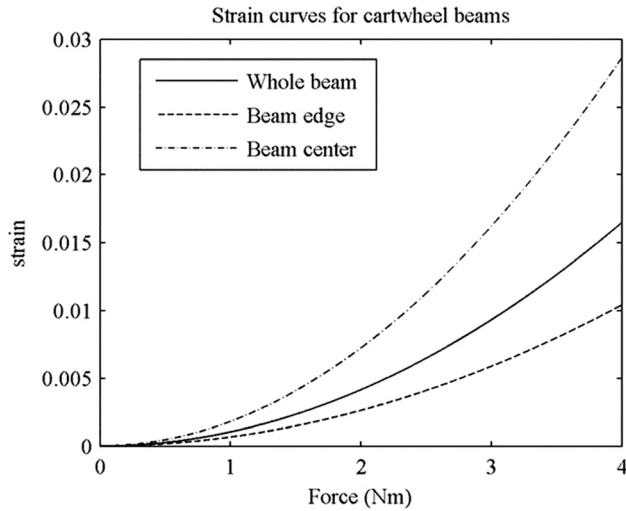
Fig. 7 Strain distribution along cartwheel flexure beam

Fig. 8 Common Wheatstone bridge circuit

[9,10,13]. The first, in Fig. 5(a), has four simple beams of width 0.25″ and thickness 0.05″, arranged circumferentially, and could withstand a maximum torque of 7 Nm. The design seen in Fig. 5(b) extended the effective length of the flexures and also led to increased rotational compliance, resulting in an increased signal-to-noise ratio. The third cartwheel flexure design is shown in Fig. 5(c), and as predicted by FEA, the effective thickness of the flexure beams was doubled so the mechanism would be able to withstand increased loads.

Table 1 shows the expected behavior of the three cartwheel flexure designs according to simulations done with COSMO-WORKS™, using 6061 Aluminum. Designs 2 and 3 improved on the desired behavior of the cartwh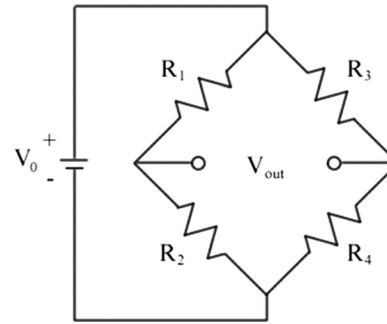eel flexure by nesting the flex-ure blades. Figures 6(a)–6(c) show the simulated von Mises stress experienced by the flexure blades at their point of failure.

2.4 Sensing. The maximum strain on the flexure blades is measured by Omega single-axis strain gauges. For the measure-ments presented in this paper, SGD-5/LY-13 strain gauges with resting resistance 350 Ω and gauge factor 2.02 were used. The strain gauges relate measured strain to a resistance change accord-ing to Eq. (3).

$$\left(\frac{\Delta R}{R_G}\right) = F_g \varepsilon \tag{3}$$

Gauges were bonded to the flexures by hand in these iterations. Figure 7 shows the expected strain along different portions of the cartwheel flexure beam. For the analysis in this paper, the gauges were affixed as close to the end of the beams as possible. Strain gauge output is converted to a voltage by a Wheatstone bridge cir-cuit, shown in Fig. 8, to compensate for both dc offset and thermal errors [9]
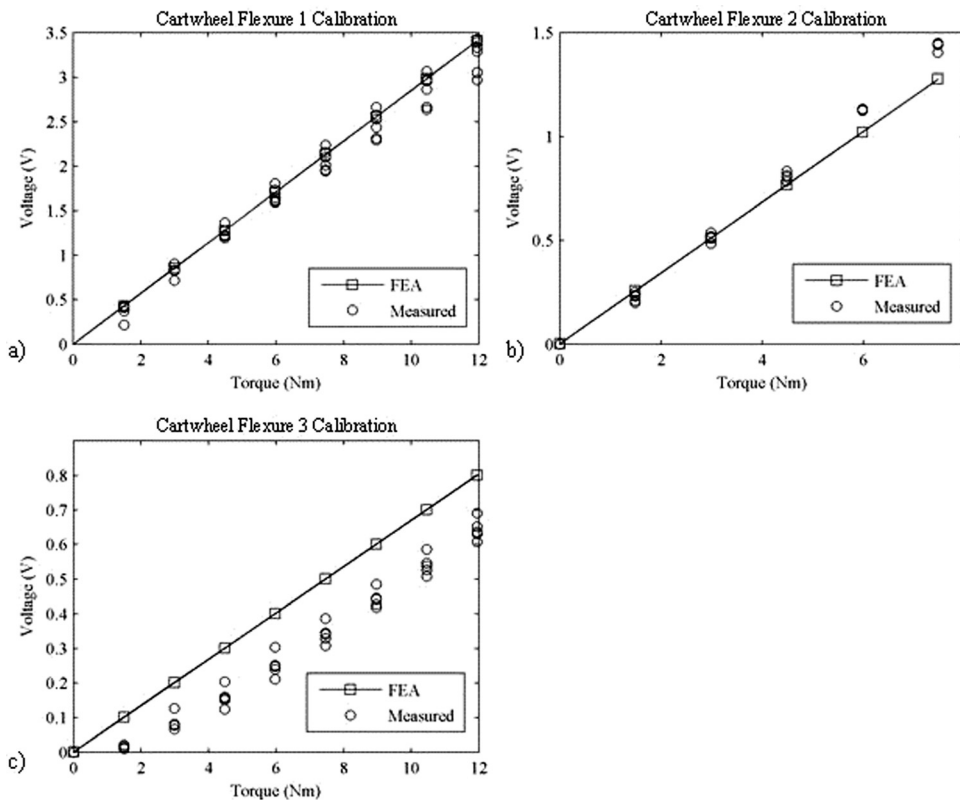

Fig. 9 Calibration date for the three (1-(a), 2-(b), 3-(c)) cartwheel flexure designs
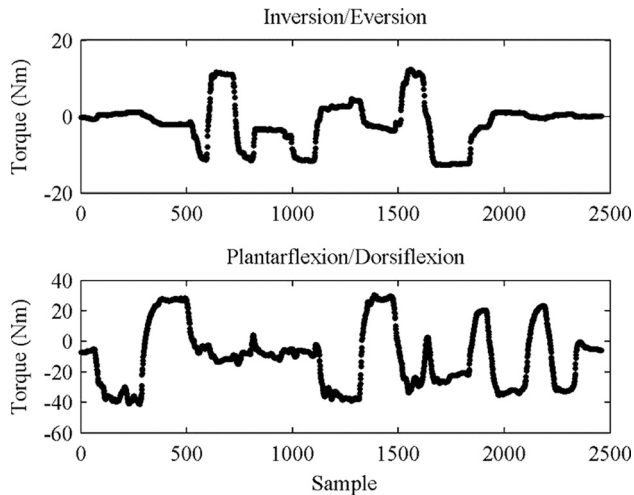
Fig. 10 Example measurement of the inversion/eversion and plantarflexion/dorsiflexion motions of the AJC

$$\frac{R_1}{R_2} = \frac{R_3}{R_4} \qquad (4)$$

$$V_{\text{out}} = \left(\frac{R_2}{R_1 + R_2} - \frac{R_4}{R_3 + R_4} \right) V^+ \qquad (5)$$

$$V_{\text{out}} = \left(\frac{2\Delta R}{R_1 + R_2} \right) V^+ \approx F_g \varepsilon V^+ \qquad (6)$$

The advantages provided by the two modified cartwheel flexures, however, are essential for the ankle rehabilitation device to satisfy its functional requirements. For any given load, resistive components R_1 and R_4 need to have the same behavior (either compression or extension), while components R_3 and R_2 both need to have opposing behavior (either extension or compression) to R_1 and R_4. At rest, the circuit should output $0\,\text{V}$, as the individual resistances of all four resistive components should be equal

$$V_{\text{out}} = \left(\frac{R_2 + R_S}{R_2 + R_S + R_1} - \frac{R_4 + R_S}{R_4 + R_S + R_3} \right) V^+ \qquad (7)$$

$$V_{\text{out}} = \left(\frac{2(\text{GF})\varepsilon}{2R_G + R_S} \right) V^+ \qquad (8)$$

$$V_2 = \left(\frac{2(\text{GF})\varepsilon}{2R_G + R_{S1}} \right) V^+ \left(\frac{2R_G + R_{S1}}{2R_G + R_{S2}} \right) = K V_1 \qquad (9)$$

To eliminate errors from the manufacturing process or gauge placement, a variable resistor of small resistance is added in series to the R_4 resistive component. Additionally a static resistor of half that small resistance is added in series to the R_2 resistive component. In the unloaded state, the variable resistor is adjusted to drive the circuit output voltage to zero. Equations (7) and (8) show the modified relation between voltage output and resistor selection, and Eq. (9) shows that the selection of the compensating resistor only affects the final output linearly by a constant factor.

3 Results

The experimental calibration setup from Fig. 4(b) was used to characterize the cartwheel flexures. By varying the calibrated weight at the end of a fixed beam, an accurate relationship between applied load and voltage was measured. Figures 9(a)–9(c) display calibration measurements taken for the three cartwheel flexure designs. Initial measurement shows that a linear relationship exists between the applied torque and output voltage for cartwheel flexure designs 1 and 2. Topological asymmetry in the third cartwheel flexure design initially suggested a nonlinear relationship below a load of 5 Nm. However, the relationship is

linear at higher loads, which it is designed to withstand, thus measurements are assumed to be linear.

The first cartwheel flexure design shows a 6% error between the measured and predicted behavior. The second cartwheel flexure design shows 14% error between its measured and expected stiffness; the displacement measured is larger than predicted, indicating that range-of-motion is greater than what the FEA predicts. The opposite is true for the third cartwheel flexure design, which shows a 16% error between measured and predicted behavior. This design deflects less under a given load, meaning it has a higher stiffness and load capacity than expected.

4 Conclusions and Future Work

For applications involving smaller radial displacements, the cartwheel flexure is especially effective in providing torque feedback. It has been demonstrated to do so accurately and precisely in a device for the diagnosis of ankle injuries. It is shown in use in Fig. 1(a); Figure 10 shows torque measurements taken with the device, illustrating coupling of AJC motion and quantitatively verifying current qualitative observations. Plantarflexion and dorsiflexion are consistently coupled with inversion and eversion, respectively. This is due to test subjects natural inclination for compound motion in the AJC, and driven by the natural biomechanics of the joint. At present, the cartwheel flexure mechanism is being utilized to simultaneously evaluate the strength and range of motion capabilities of the human ankle joint complex for diagnostic and rehabilitative purposes [2,14].

The radial displacement exhibited by the cartwheel flexure is ideal for combining evaluations of both range of motion and force in diagnostic and rehabilitative applications. Current technology is unable to simultaneously measure range-of-motion and applied load. Further experimental results in four test subjects were used to validate the initial hypothesis of simultaneously measuring load and range-of-motion [14].

References

[1] Paros, J. M., and Weisbord, L., 1965, "How to Design Flexure Hinges," Mach. Des., **37**(27), pp. 151–156.
[2] Ma, R., Slocum, A., Sung, E., Culpepper, M., and Bean, J., 2010, "Ankle Rehabilitation via Compliant Mechanisms," Design of Medical Devices Conference, Apr. 13–15, Minneapolis.
[3] Smith, S., 2000, *Flexures: Elements of Elastic Mechanisms*, Gordon and Breach Science Publishers, Newark, NJ.
[4] Lobontiu, N., 2002, *Compliant Mechanisms: Design of Flexure Hinges*, CRC Press, Boca Raton.
[5] Dibiasio, C., Culpepper, M., Panas, R., Howell, L., and Magleby, S., 2008, "Comparison of Molecular Simulation and Pseudo-Rigid-Body Model Predictions for a Carbon Nanotube-Based Compliant Parallel-Guiding Mechanism," J. Mech. Des., **130**(4), p. 042308.
[6] Pei, X., Yu, J., Zong, G., Bi, S., and Su, H., 2009, "The Modeling of Cartwheel Flexural Hinges," Mech. Mach. Theory, **44**, pp 1900–1909.
[7] Shushen, B., Hongzhe, Z., and Jingjun, Y., 2009, "Modeling of a Cartwheel Flexural Pivot," J. Mech. Des., **131**, p. 061010.
[8] Vischer, D., and Khatib, O., 1995, "Design and Development of High-Performance, Torque-Controlled Joints," Rob. Autom., **11**(4), pp. 537–544.
[9] Hirzinger, G., Albu-Schaffer, A., Hahnle, M., Schaefer, I., and Sporer, N., 2001, "New Generation of Torque Controlled Light-Weight Robots," International Conference on Robotics and Automation, pp. 3356–3363.
[10] Ahili, F., Buehler, M., and Hollerbach, J., 2001, "Design of a Hollow Hexaform Torque Sensor for Robot Joints," Int. J. Rob. Res., **20**(12), pp. 967–976.
[11] Young, W. C., and Budynas, R. C., 2002, *Roark's Formulas for Stress and Strain*, 7th ed., McGraw-Hill, New York.
[12] Trease, B., Moon, Y., and Kota, S., 2005, "Design of Large-Displacement Compliant Joints," J. Mech. Des., **127**(4), p. 788.
[13] Diddens, D., Reynaerts, D., and Brussel, H., 1995, "Design of a Ring-Shaped Three-Axis Micro Force/Torque Sensor," Sens. Actuators, **46**, pp. 225–232.
[14] Sung, E., Slocum, A. H., Jr., Ma, R., Bean, J. F., and Culpepper, M. L., 2011, "Design of an Ankle Rehabilitation Device Using Compliant Mechanisms," ASME J. Med. Devices, **5**, p. 011001.